ACS OMEGA

Open Access

This article is licensed under CC-BY-NC-ND 4.0

http://pubs.acs.org/journal/acsodf

Article

Role of Oxygen in Amorphous Carbon Hard Mask Plasma Etching

Hee-Jung Yeom, Min Young Yoon, Daehan Choi, Youngseok Lee, Jung-Hyung Kim,* Shin-Jae You,* and Hyo-Chang Lee*

Cite This: *ACS Omega* 2023, 8, 32450−32457

Read Online

ACCESS | Metrics & More | Article Recommendations | Supporting Information

ABSTRACT: In the current and next-generation Si-based semiconductor manufacturing processes, amorphous carbon layer (ACL) hard masks are garnering considerable attention for high-aspect-ratio (HAR) etching due to their outstanding physical properties. However, a current limitation is the lack of research on the etching characteristics of ACL hard masks under plasma etching conditions. Given the significant impact of hard mask etching on device quality and performance, a deeper understanding of the etching characteristics of ACL is necessary. This study aims to investigate the role of oxygen in the etching characteristics of an ACL hard mask in a complex gas mixture plasma etching process. Our results show that a small change of oxygen concentration (3.5−6.5%) can significantly alter the etch rate and profile of the ACL hard mask. Through our comprehensive plasma diagnostics and wafer-processing results, we have also proven a detailed mechanism for the role of the oxygen gas. This research provides a solution for achieving an outstanding etch profile in ACL hard masks with sub-micron scale and emphasizes the importance of controlling the oxygen concentration to optimize the plasma conditions for the desired etching characteristics.

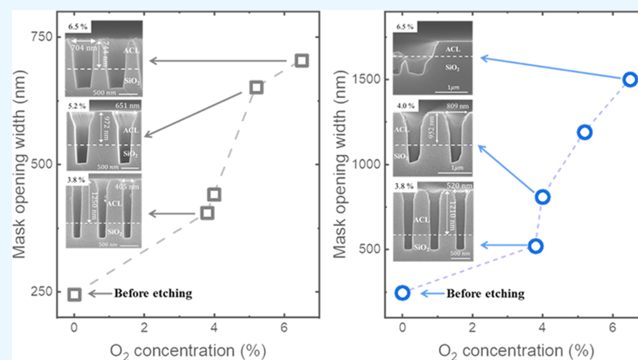

1. INTRODUCTION

The trend in the electronics industry toward miniaturization continues to drive the development of nanoscale electronic devices. This is due to the growing demand for compact, fast-performing and energy-efficient devices that offer high levels of integration.[1−6] The International Technology Roadmap for Semiconductors[7] predicts that by 2034 the critical feature size of logic devices will be below 10 nanometers and that three-dimensional (3D) devices will have over 512 layers for 3D NAND flash. In addition, the maximum bit density is expected to increase fivefold between 2018 and 2028, further augmenting the capabilities of nanoelectronic devices. As a result, the advancement of nanoelectronic devices necessitates the utilization of increasingly complex semiconductor fabrication methodologies. Therefore, the advancement of the nanoelectronic device industry demands the implementation of highly advanced semiconductor etching technologies.

Accordingly, in the modern semiconductor etching process, especially high-aspect-ratio (HAR) etching, harsher plasma process conditions such as high ion bombardment energy and complex chemical reactions are required to form narrow and deep patterns.[8−10] However, these harsh conditions may result in damage to the photoresist or hard mask, thereby affecting the etch result of the underlying layer. Si-based conventional single-layer hard masks such as silicon oxide[11] and silicon nitride[11,12] are frequently used to provide protection during the etching process. However, there are several drawbacks associated with these hard masks, including limited selectivity, mask erosion, mask undercutting, wiggling, and pattern collapse in the high ion energy condition due to low plasma resistivity.[13−17] The damage to the hard mask is directly related to the process yield because it affects the etching shape and depth of the pattern. Therefore, to overcome these challenges and enhance device performance and yield, alternative hard mask materials and processes are being developed.

The application of amorphous carbon as an alternative hard mask for conductive or dielectric underlayer HAR etching has been introduced as a means of addressing the limitations associated with conventional single-layer hard masks based on silicon.[18−26] The utilization of an amorphous carbon layer (ACL) as an etching mask in nanoscale plasma etching patterning is facilitated by its impressive physical properties, including a high melting point, exceptional hardness, and resistance to corrosion and etching in Cl- or F-containing gases. Additionally, in both current and next-generation semiconductor processing, the ACL hard mask, in conjunction with a complex gas mixed plasma, can be leveraged to achieve

Received: April 11, 2023
Accepted: July 20, 2023
Published: August 31, 2023

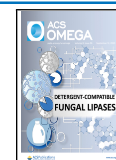

© 2023 The Authors. Published by American Chemical Society

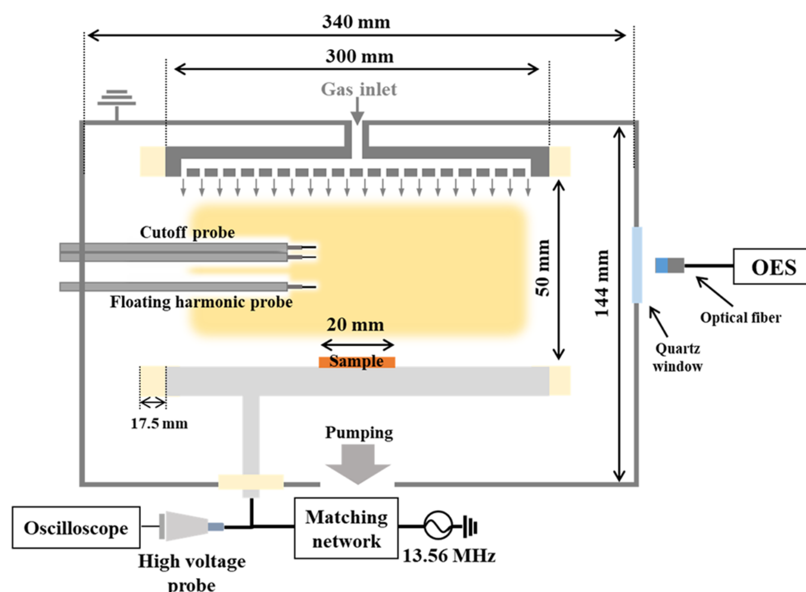

Figure 1. Schematic diagram of the experimental setup.

high etching selectivity in HAR etching.[27−29] In industrial semiconductor plasma etching, three or more complex gas mixtures, which are based on inert gases such as argon and composed of a combination of oxygen, C_xF_y, and $C_xH_yF_z$ gases, are used to control the etch profile and selectivity.[30,31] In a complex gas mixture, inert gas is injected to control the plasma density and degree of dissociation rate,[32] and a trace amount of oxygen gas is injected to control the degree of precursors and deposited polymers produced in the plasma.[30,33] However, the high removability of the ACL by oxygen can result in unwanted sidewall etching of the ACL hard mask when exposed to a processing plasma containing oxygen gas, leading to a distorted etch profile and increased pattern opening. Thus, it is imperative to analyze and regulate the etching characteristics of the ACL when using oxygen gas as the profile of the hard mask holds a significant influence on the profile of the bottom layer to be etched, and thus greatly impacts the device quality and performance..[22,34]

However, even though the etch characteristics of the ACL hard mask, such as etch rate, etch profile of mask, and mask damage (wiggling, notching, and pattern collapse) may differ caused by the small amount of oxygen gas and inert gas species, prior studies have focused on the etching characteristics of conductive or dielectric underlayers and not on those of the ACL mask. In addition, studies on the etch properties (etch rate, damage, and etch selectivity) of ACL hard masks have been scarce in plasma etching technologies, despite their importance in the manufacturing process of current and next-generation devices, such as 3D DRAM and vertical-NAND flash memory with high-aspect-ratio patterns. Furthermore, current and next-generation semiconductor manufacturing involves the use of complex gas mixtures based on Kr or Xe plasma, as well as Ar plasma, for HAR etching processes.[35,36] Therefore, it is imperative to investigate the effects of trace amounts of oxygen on the ACL hard mask, which are contingent upon the species of inert gas utilized.

In this study, we studied the etching characteristics of ACL due to both inert gas species and trace amounts of oxygen. It was found that the etch rate of ACL hard masks increases dramatically with increasing O_2 concentration, although it varies minimally (4−6.5%) in fluorocarbon-mixed gas plasmas. The effect of inert gas species (Ar, Kr, and Xe) on the etch rate and profile of the ACL was studied. These results were compared with the measured plasma parameters, such as electron density (n_e), electron temperature (T_e), optical emission intensity of atomic oxygen, and electrode voltage related to ion energy under various discharge conditions. Finally, excellent etch profiles of the bottom layer with less ACL hard mask damage were obtained through flow rate control of oxygen and the fluorocarbon-based gas through these comprehensive studies. As a result, we developed a technology that can control the etch profile of the ACL hard mask by adjusting a small amount of oxygen gas flow rate at a level where plasma parameters involved in etching, such as electron temperature and ion energy, hardly change.

2. MATERIALS AND METHODS

2.1. Experimental Setup. The etching process was performed using a capacitively coupled plasma (CCP), which is widely used in industrial semiconductor processes. The chamber geometry, radio-frequency power feeding, and plasma diagnostic system are shown in Figure 1. The chamber was cylindrical with an inner diameter of 340 mm and a height of 50 mm from the top to the bottom electrode. The 13.56 MHz power supply connected to the bottom electrode with the wafer through an L-type auto-matcher provided an input power of 500 W during the experiment. The surfaces of the powered electrode and the ground electrode were coated with Al_2O_3. The gases used in this experiment were Ar, O_2, C_4F_8, and CH_2F_2. The flow rates of Ar, C_4F_8, and CH_2F_2 were 60, 6, and 6 sccm, respectively. The flow rate of O_2 gas was increased from 3 to 5 sccm, which accounted for 4−6.5% of the total gas flow rate. The condition of oxygen concentration below 4% was achieved by adjusting the flow rate of the inert gas or the fluorocarbon gas. Kr and Xe gases were used to observe the effects of changes in inert gas species and O_2 gas flow rates on the plasma parameters, etch rate, and etch profile. Rotary and turbomolecular pumps were employed to maintain a background pressure of 5×10^{-6} Torr, measured using a Penning

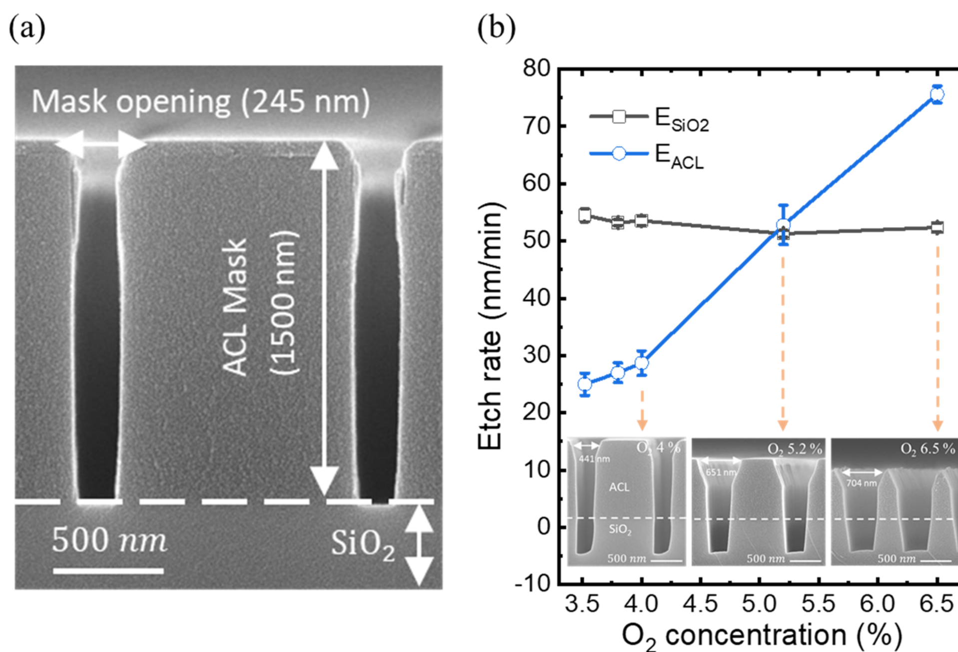

Figure 2. FE-SEM image of the patterned wafers etched for 10 min with Ar-based mixture plasma: (a) reference sample mask opening width of 245 nm, and (b) etch rates of SiO_2 and ACL as a function of the O_2 concentration under an input power of 500 W and gas pressure of 28 mTorr.

gauge. The experimental pressure was 28 mTorr, measured using a capacitive manometer.

A microwave cutoff probe was employed to measure the electron density (n_e),[37,38] whereas a floating harmonic probe was used to measure the electron temperature (T_e).[39,40] Both probes were placed at the center of the discharge chamber (25 mm above the powered electrode) to measure the plasma parameters at the same measurement position. The microwave cutoff probe was connected to a network analyzer (*SALUKI*, S3601) via 50 Ω coaxial cables to obtain the transmission spectrum. An optical emission spectrometer (OES, *Ocean optics*, HR 4000) installed on a quartz window located 25 mm above the bottom electrode was used to measure the emission spectrum of the plasma bulk. A high-voltage probe (*Tektronix*, P6015A) was connected between the matcher and the bottom electrode to measure the DC self-bias voltage (V_{DC}) at the electrode. In this experiment, a wafer with trench patterns was prepared on a stack of ACL (1500 nm)/SiO_2 (2000 nm)/Si substrates. The patterned wafer was manufactured by a chip-maker of a memory semiconductor. The ACL hard mask was deposited within a low-pressure regime of a plasma-enhanced chemical vapor deposition chamber, utilizing C_2H_2 gas as the carbon source and a combination of Ar, N_2, and He gases, as documented in ref 41, 42. The width of the ACL hard mask opening was 245 nm. The etch rate and profile of the patterned wafer were measured using field-emission scanning electron microscopy (FE-SEM, *Hitachi*, S-4800).

2.2. Plasma Diagnostic Method. The microwave cutoff probe is the plasma diagnostic method that measures the absolute electron density based on the transmission of the minimum electromagnetic wave from the radiating antenna to the detecting antenna. The physics behind the cutoff probe was clarified by Kim et al.[37,38] The dispersion relation of electromagnetic waves propagating in a plasma with no DC magnetic field or of an ordinary wave in a DC magnetic field is given by $\omega^2 = \omega_{pe}^2 + c^2k^2$, where ω is the frequency of the electromagnetic wave, ω_{pe} is the electron plasma frequency, c is the speed of light, and k is the wave number. When an electromagnetic wave radiating from the radiating antenna is lower than the cutoff frequency of the plasma, the wave is generally reflected and can no longer propagate at the cutoff. The relation between the cutoff frequency and electron density is given by $n_e = \omega_{pe}^2 \epsilon_0 m_e / e^2$, where ϵ_0 is the vacuum permittivity, e is the elementary charge, and m_e is the electron mass. The cutoff method provides high accuracy (uncertainty under 2%)[43,44] in the measurement of absolute electron density due to its simple equation without any specific assumptions.

The floating harmonic probe is a plasma diagnostic method.[39] A voltage of the kHz frequency band is applied to the metal tip, and it measures the ion flux and electron temperature by analyzing the current coming into the probe tip through the sheath. The current flow through the probe tip when the electrons are in the Maxwellian distribution is given by $i_{pr} = 2i^- \exp\left[\frac{e(\overline{V} - V_p)}{T_e}\right][i_{1\omega} + i_{2\omega} + \cdots]$, where i^- is the electron saturation current, T_e is the electron temperature, $\overline{V}$ is the DC bias voltage, V_p is the plasma potential, ω is the frequency applied to the probe, and $i_{n\omega}$ is the nth harmonic current. The electron temperature can be obtained by the ratio of any two harmonic current amplitudes. The ratio of the amplitudes of the first and second harmonics is given by $|i_{1\omega}|/|i_{2\omega}| = I_1\left(\frac{eV_0}{T_e}\right)/I_2\left(\frac{eV_0}{T_e}\right)$, where V_0 is the RF voltage amplitude of the applied voltage and I_n is the current amplitude of the nth harmonic current. The ion flux is given by $i_{1\omega} = 2(0.61en_iu_BA)(I_1/I_0)\cos(\omega t)$, where n_i is the ion density, u_B is the Bohm velocity, and A is the probe area.

3. RESULTS AND DISCUSSION

The etch rate and etch selectivity of SiO_2 to the ACL hard mask were measured by varying the O_2 concentration in the $Ar/O_2/C_4F_8/CH_2F_2$ plasma. During these experiments, the input power, gas pressure, and etching time were maintained at

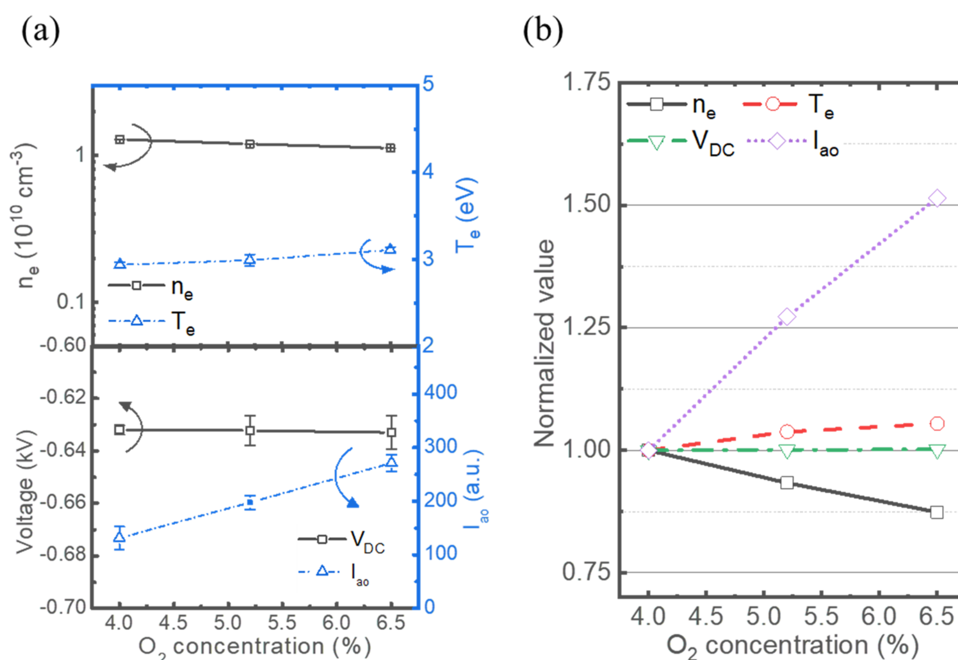

Figure 3. Results for argon: measured plasma parameters (a) n_e, T_e, V_{DC}, and I_{ao} and (b) normalized values of n_e, T_e, V_{DC}, and I_{ao} as a function of O_2 concentration under an input power of 500 W, gas pressure of 28 mTorr, and Ar, C_4F_8, and CH_2F_2 of 60, 6, and 6 sccm condition, respectively.

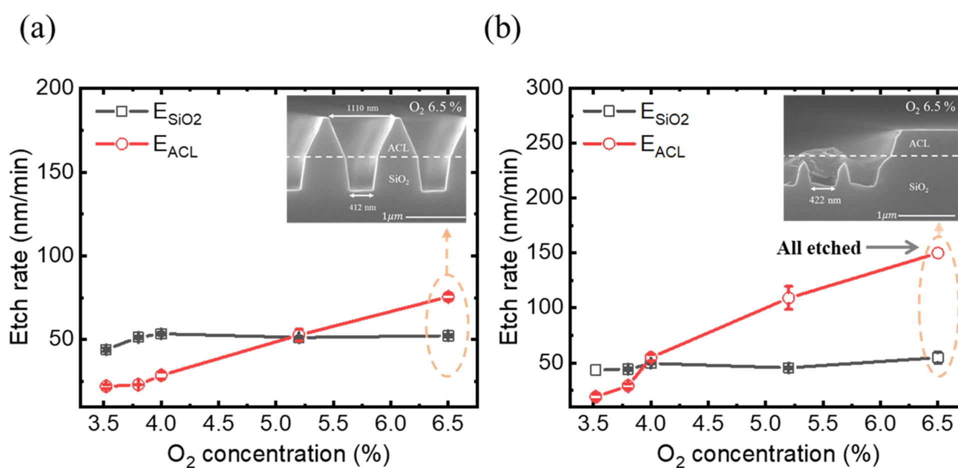

Figure 4. SiO_2 and ACL etch rate results for (a) Kr and (b) Xe as a function of the O_2 concentration under an input power of 500 W and gas pressure of 28 mTorr.

500 W, 28 mTorr, and 10 min, respectively. Figure 2a shows the cross-sectional FE-SEM image of the reference sample (mask opening width: 245 nm) and Figure 2b shows the etch rates of SiO_2 (E_{SiO_2}), ACL hard mask (E_{ACL}), and the cross-sectional views of the after-etching process depending on the concentration of O_2. As shown in Figure 2b, when the O_2 gas concentration increased from 3.5 to 6.5%, the E_{ACL} increased from 25 to 76 nm/min, whereas the E_{SiO_2} was constant. The etch selectivity of SiO_2 for ACL decreased from 2.18 to 0.8. It is possible to confirm the significant change in the etching rate of ACL due to the increase in O_2 flow rate when the O_2 fraction is above 4% through Figure 2b. Therefore, we conducted plasma measurements under conditions with O_2 fraction exceeding 4%.

The etching characteristics in the Ar-based mixture plasma were analyzed by measuring the plasma parameters according to the change in the concentration of O_2 gas. Figure 3a shows the results for the plasma parameters under Ar-based mixture plasma conditions. As the concentration of O_2 gas increased, n_e decreased slightly from 1.24×10^{10} to 1.18×10^{10} cm^{-3} and T_e increased slightly from 2.9 to 3.2 eV. This is because the absorbed power is additionally dissipated by energy loss as a result of the dissociation and vibrational/rotational motion of the molecular gas and the increase in electronegativity of the gas discharge.[45−48] The V_{DC} increased as the concentration of O_2 gas increased, as shown in Figure 3a. The change in V_{DC} with O_2 concentration is due to the decreased electron density leading to decreased plasma conductivity. Here, the plasma conductivity is given by $\sigma_p = \frac{\epsilon_0 \omega_{pe}^2}{j\omega + \nu_m}$, where ϵ_0 is the vacuum permittivity, ω_{pe} is the electron plasma frequency, ω is the driving frequency, and ν_m is the electron-neutral collision frequency.[49] This variation of V_{DC} is directly related to the ion energy, which causes ACL and SiO_2 sputtering and damage as the O_2 gas concentration increases. The optical emission

https://doi.org/10.1021/acsomega.3c02438
ACS Omega 2023, 8, 32450−32457

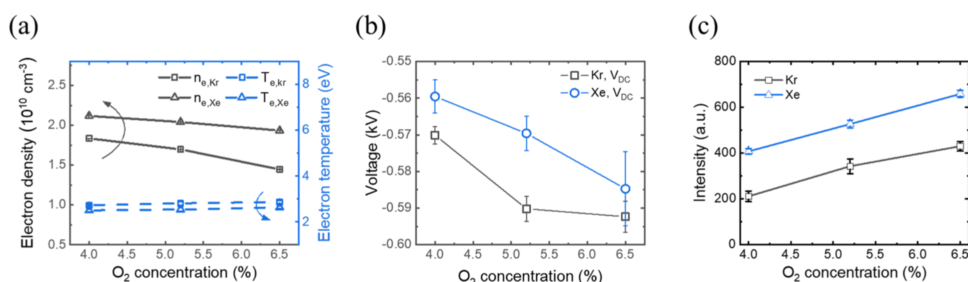

Figure 5. Results obtained using Kr and Xe. Plots of the measured plasma parameters (a) n_e and T_e, (b) V_{DC}, and (c) I_{ao} as functions of the O_2 concentration under an input power of 500 W, gas pressure of 28 mTorr, and inert gas, C_4F_8, and CH_2F_2 of 60 sccm, 6 sccm, and 6 sccm condition, respectively.

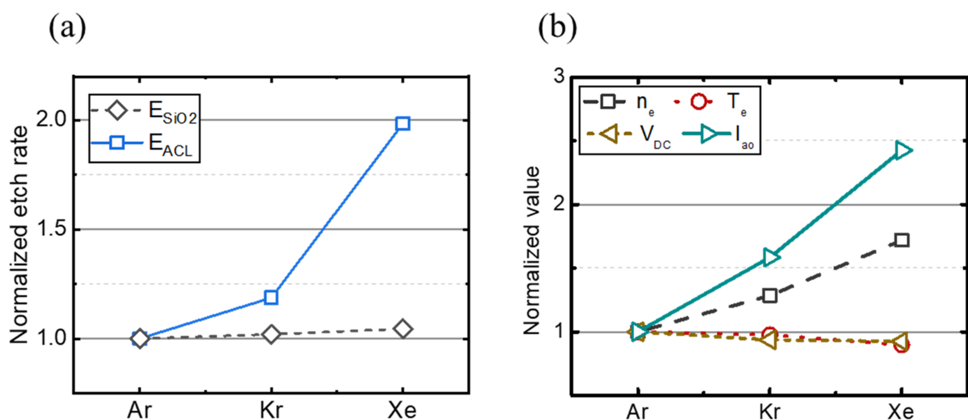

Figure 6. Normalized values of (a) E_{SiO_2} and E_{ACL} and (b) measured n_e, T_e, V_{pp}, V_{DC}, and I_{ao} depending on the inert gas species when the O_2 concentration is 6.5% under an input power of 500 W, gas pressure of 28 mTorr, and inert gas, C_4F_8, and CH_2F_2 of 60 sccm, 6 sccm, and 6 sccm condition, respectively.

intensity of atomic oxygen (I_{ao}) at the 3p5P → 3s5S state transition (777.4 nm)[50] was measured using OES. The I_{ao} is proportional to oxygen radical density, and an oxygen radical is known to be the main etchant of carbon-based materials.[41] The oxygen radical is highly reactive with the carbon atoms on the ACL surface to produce volatile low-weight molecular species such as CO and CO_2. Reactions of carbon atoms with oxygen are as follows:[51,52] $C(g) + O_2 \rightarrow CO_2(g)$, $C(g) + O_2 \rightarrow CO(g) + O$, $C + O \rightarrow CO(g), CO_2(g)$.

In this experiment, I_{ao} increased approximately twofold from 131 to 272. This increase in I_{ao} indicates an increase in the etchant of ACL, and it causes an increased etch rate of the ACL hard mask and an isotropic etch profile by chemical reaction. Figure 3b shows the measured plasma parameters, normalized at a discharge condition of 4% O_2 concentration. The T_e and V_{DC} did not significantly change as the flow rate of oxygen increased; however, n_e decreased by approximately 12% and I_{ao} increased twofold. This implies that the change in E_{ACL} characteristics mainly arises from the increase in O radicals.

To investigate the change in etching characteristics according to the inert gas species involved, more experiments were performed using inert gases, such as Kr and Xe, instead of Ar. The experiments were performed under the same discharge conditions as those used for the Ar mixture plasma. Figure 4 shows the etch results obtained using Kr and Xe mixture plasmas. Figure 4a shows the E_{ACL}, E_{SiO_2}, and the cross-sectional FE-SEM image of the after-etching process using the Kr mixture plasma, and Figure 4b shows the E_{ACL}, E_{SiO_2}, and the cross-sectional view of the after-etching process using the Xe mixture plasma, depending on the O_2 concentration. In Figure 4, the E_{SiO_2} under the Kr and Xe mixture plasma conditions hardly changed, even when the concentration of oxygen was slightly increased (44−52 nm/min). However, the E_{ACL} changed dramatically, increasing from 22 to 75 nm/min for the Kr mixture and from 19 to 150 nm/min (all-etched) for the Xe mixture, as the concentration of O_2 increased. Accordingly, the SiO_2/ACL selectivity decreased from 1.99 to 0.73 in the case of the Kr mixture plasma and from 2.26 to 0.36 for the Xe mixture plasma as the O_2 concentration increased. In the case of the 6.5% of O_2 concentration, the mask opening width was surprisingly 4.5 times wider than that of the reference sample (see Figure 2a) for the Kr mixture plasma, and all ACL masks were etched under the Xe-based mixture plasma. In addition, compared to the results obtained for Ar, the mask opening width increased 1.57 times for the Kr mixture in the 6.5% O_2 condition. Figure 5 shows the measured plasma parameters as the O_2 concentration increased in the Kr and Xe mixture plasmas. Similar to the results for the Ar mixture plasma, n_e decreased as the O_2 concentration increased, and T_e and V_{DC} tended to increase slightly. In addition, the I_{ao} also increased as the O_2 concentration increased. Therefore, it is shown that the increase in E_{ACL} with increasing O_2 concentration is the main effect of the increase in O radicals.

Although the change in the etch characteristics according to the O_2 gas ratio can be explained by the change in the O radical, the variations in the etch characteristics depending on the inert gas species need to be analyzed more thoroughly. For this reason, it is necessary to examine the variations in plasma

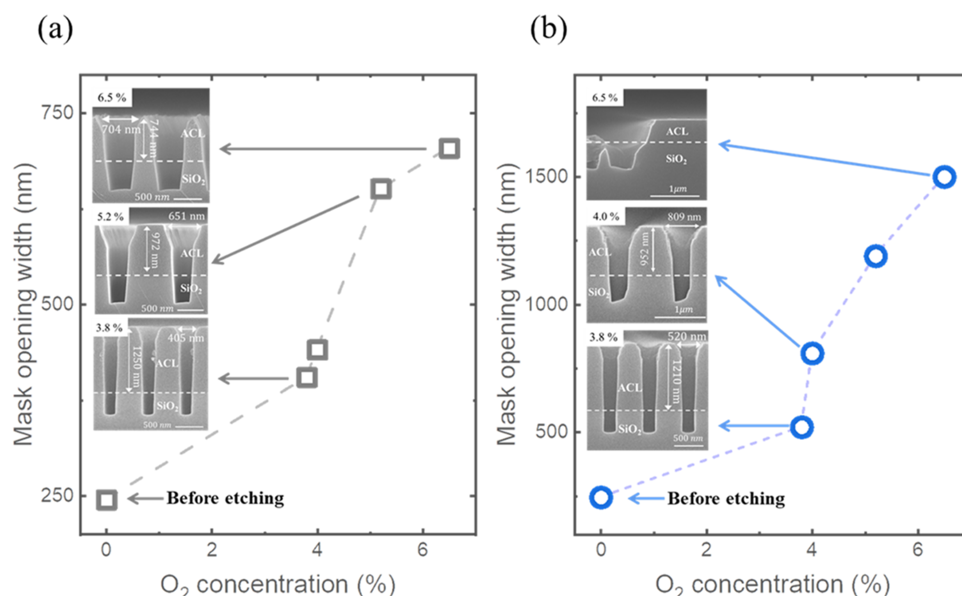

Figure 7. FE-SEM image and the mask opening width of (a) Ar-based mixture plasma and (b) Xe-based mixture plasma depending on O_2 concentration under an input power of 500 W and gas pressure of 28 mTorr.

parameters as the inert gas species change. Figure 6 shows the normalized values of the etch rate (Figure 6a) and plasma parameters (Figure 6b) when the concentration of O_2 is 6.5%. In Figure 6a, E_{SiO_2} does not change with changes in the inert gas species; however, the E_{ACL} changes by more than a factor of two. Notably, the optical emission of O radicals increased linearly; however, the E_{ACL} tended to increase significantly when the inert gas was changed from Kr to Xe. This could be understood as a synergistic effect of the chemical and physical reactions. In Figure 6b, T_e and V_{DC} decrease slightly as the mass of the inert gas (Ar: 40 amu, Kr: 83 amu, and Xe: 131 amu) increases. However, n_e increased 1.28 times in Kr and 1.72 times in Xe, compared to the n_e variation in Ar. The increase in n_e in Kr and Xe gases is attributed to the reduced ionization threshold energy and collisional energy loss per electron−ion pair creation.[53] As n_e increases, the ion density increases owing to the quasi-neutrality of the plasma and thus the sputtering of the ACL hard mask is expected to increase. In addition, as the mass of the inert gas increases, I_{ao} also increases due to the enhanced n_e. Therefore, the dramatic change in E_{ACL} is considered to be a synergistic effect involving not only O radicals but also ion density.

The ACL mask distortion caused by the O_2 concentration can be controlled by lowering the ratio of O_2 gas and adding a fluorocarbon-based gas that reacts with O radicals. Thus, we optimized the process recipe by applying the reduced O_2 gas fraction in the mixture gas: 60 sccm of inert gas flow rate, 7.5 sccm of CH_2F_2 and C_4F_8 gas flow rate, and 3 sccm of O_2 gas flow rate. Figure 7a,b shows the cross-sectional FE-SEM image of the after-etching process using the Ar-based and Xe-based mixture plasmas under the 3.8% O_2 condition, respectively. In Figure 7a, the mask opening width decreased by 34 nm compared with the 4% O_2 condition, and the pattern height was less etched by 30 nm in the Ar-based mixture plasma. In the Xe-based mixture plasma (see Figure 7b), the mask opening width decreased by 289 nm compared with the 4% O_2 condition, and the pattern height was etched less by 90 nm. As the O_2 gas fraction increased, the mask opening width increased, which was more dramatic as the inert gas mass increased. In addition, the mask opening width was greatly reduced when the O_2 concentration was decreased and the fluorocarbon-based gas flow rate increased. In conclusion, an outstanding etch profile in the ACL hard mask with sub-micron scale can be obtained while reducing the damage to it through the selection of gas species that can consume O radicals and through precise gas flow rate control.

4. CONCLUSIONS

In this study, the effects of varying O_2 gas concentrations with the same input power and gas pressure on the etch selectivity of an ACL hard mask and SiO_2 underlayer in Ar, Kr, and Xe/O_2/C_4F_8/CH_2F_2 mixture plasmas were investigated. It was confirmed that the ACL etch rate and etch profile changed significantly with a slight change in the concentration of O_2 (3.5−6.5%). Furthermore, the ACL etch rate increased and the profile trend became more distorted as the mass of the inert gas increased. In addition, the density of O radicals and n_e were found to be important parameters for the E_{ACL} and etch profiles using plasma diagnostics. Based on these process and plasma diagnosis results, the etch process conditions, in which the distortion of the ACL hard mask is strongly reduced and the anisotropic etching profile of the bottom layer is represented, were derived by lowering the mixture ratio of the O_2 gas. These results for the plasma parameters and etch characteristics are expected to aid the search for a new industrial etching process technology in current and next-generation semiconductor fabrication.

■ ASSOCIATED CONTENT

Supporting Information

The Supporting Information is available free of charge at https://pubs.acs.org/doi/10.1021/acsomega.3c02438.

Additional figure presents data obtained by measuring the surface of the ACL hard mask using energy-dispersive X-ray spectroscopy (EDS) to confirm the presence of re-deposition caused by sputtering of the electrode material. The measurements were conducted under the following conditions: an input power of 500

https://doi.org/10.1021/acsomega.3c02438
ACS Omega 2023, 8, 32450−32457

W, a gas pressure of 28 mTorr, and flow rates of Xe, O_2, C_4F_8, and CH_2F_2 set at 60, 5, 6, and 6 sccm, respectively (PDF)

AUTHOR INFORMATION

Corresponding Authors

Jung-Hyung Kim − *Korea Research Institute of Standards and Science, Daejeon 34113, Republic of Korea*; Email: jhkim86@kriss.re.kr

Shin-Jae You − *Department of Physics, Chungnam National University, Daejeon 34134, Republic of Korea; Institute of Quantum System (IQS), Chungnam National University, Daejeon 34134, Republic of Korea*; Email: sjyou@cnu.ac.kr

Hyo-Chang Lee − *School of Electronics and Information Engineering, Korea Aerospace University, Goyang 10540, Republic of Korea; Department of Semiconductor Science, Engineering and Technology, Korea Aerospace University, Goyang 10540, Republic of Korea*; orcid.org/0000-0003-2754-1512; Email: plasma@kau.ac.kr

Authors

Hee-Jung Yeom − *Korea Research Institute of Standards and Science, Daejeon 34113, Republic of Korea; Department of Physics, Chungnam National University, Daejeon 34134, Republic of Korea*

Min Young Yoon − *Korea Research Institute of Standards and Science, Daejeon 34113, Republic of Korea*

Daehan Choi − *Korea Research Institute of Standards and Science, Daejeon 34113, Republic of Korea*

Youngseok Lee − *Institute of Quantum System (IQS), Chungnam National University, Daejeon 34134, Republic of Korea*

Complete contact information is available at: https://pubs.acs.org/10.1021/acsomega.3c02438

Notes

The authors declare no competing financial interest.

ACKNOWLEDGMENTS

This research was supported by the Material Innovation Program (Grant No. 2020M3H4A3106004) of the National Research Foundation (NRF) of Korea and funded by (i) the Ministry of Science and ICT and the R&D Convergence Program (Grant No. CRC-20-01-NFRI) of the National Research Council of Science and Technology (NST) of the Republic of Korea; (ii) the Korea Evaluation Institute of Industrial Technology (Grant No. 1415181740); and (iii) the Korea Research Institute of Standards and Science (Grant Nos. KRISS GP2023-0012-08, GP2023-0012-09).

REFERENCES

(1) Lill, T.; Joubert, O. MATERIALS SCIENCE: The Cutting Edge of Plasma Etching. *Science* **2008**, *319*, 1050−1051.

(2) Wu, B.; Kumar, A.; Pamarthy, S. High Aspect Ratio Silicon Etch: A Review. *J. Appl. Phys.* **2010**, *108*, No. 051101.

(3) Donnelly, V. M.; Kornblit, A. Plasma Etching: Yesterday, Today, and Tomorrow. *J. Vac. Sci. Technol., A* **2013**, *31*, No. 050825.

(4) Lee, H.-C. Review of Inductively Coupled Plasmas: Nano-Applications and Bistable Hysteresis Physics. *Appl. Phys. Rev.* **2018**, *5*, No. 011108.

(5) Lee, C. G. N.; Kanarik, K. J.; Gottscho, R. A. The Grand Challenges of Plasma Etching: A Manufacturing Perspective. *J. Phys. D: Appl. Phys.* **2014**, *47*, No. 273001.

(6) Abe, H.; Yoneda, M.; Fujiwara, N. Developments of Plasma Etching Technology for Fabricating Semiconductor Devices. *Jpn. J. Appl. Phys.* **2008**, *47*, 1435−1455.

(7) *International Roadmap for Devices and Systems (2018)*. https://irds.ieee.org/editions/2018.

(8) Yoon, M. Y.; Yeom, H. J.; Kim, J. H.; Jeong, J.-R.; Lee, H.-C. Plasma Etching of the Trench Pattern with High Aspect Ratio Mask under Ion Tilting. *Appl. Surf. Sci.* **2022**, *595*, No. 153462.

(9) Cardinaud, C.; Peignon, M.-C.; Tessier, P.-Y. Plasma Etching: Principles, Mechanisms, Application to Micro- and Nano-Technologies. *Appl. Surf. Sci.* **2000**, *164*, 72−83.

(10) Graves, D. B.; Humbird, D. Surface Chemistry Associated with Plasma Etching Processes. *Appl. Surf. Sci.* **2002**, *192*, 72−87.

(11) Wüest, R.; Strasser, P.; Robin, F.; Erni, D.; Jäckel, H. Fabrication of a Hard Mask for InP Based Photonic Crystals: Increasing the Plasma-Etch Selectivity of Poly(Methyl Methacrylate) versus SiO[Sub 2] and SiN[Sub X]. *J. Vac. Sci. Technol., B: Microelectron. Nanometer Struct.–Process., Meas., Phenom.* **2005**, *23*, 3197.

(12) Jung, J.-E.; Barsukov, Y.; Volynets, V.; Kim, G.; Nam, S. K.; Han, K.; Huang, S.; Kushner, M. J. Highly Selective Si 3 N 4 /SiO 2 Etching Using an NF 3 /N 2 /O 2 /H 2 Remote Plasma. II. Surface Reaction Mechanism. *J. Vac. Sci. Technol. A* **2020**, *38*, No. 023008.

(13) Zhang, Y.; Oehrlein, G. S.; Bell, F. H. Fluorocarbon High Density Plasmas. VII. Investigation of Selective SiO 2 -to-Si 3 N 4 High Density Plasma Etch Processes. *J. Vac. Sci. Technol., A* **1996**, *14*, 2127−2137.

(14) Namatsu, H.; Yamazaki, K.; Kurihara, K. Supercritical Drying for Nanostructure Fabrication without Pattern Collapse. *Microelectron. Eng.* **1999**, *46*, 129−132.

(15) Yang, Y.; Lee, J. H.; Kim, T. H.; Choi, S. J.; Choi, S. J.; Chang, T.; Kim, S.; Kim, D.; Kim, H.; Kim, Y.; Chae, S.-K.; Kim, J. H. Design and Development of ArF Photoresist for Implant Layers. *J. Photopolym. Sci. Technol.* **2010**, *23*, 259−264.

(16) Simons, J. P.; Goldfarb, D. L.; Angelopoulos, M.; Messick, S.; Moreau, W. M.; Robinson, C.; de Pablo, J. J.; Nealey, P. F. Image Collapse Issues in Photoresist, SPIE Proceedings; Houlihan, F. M., Ed.; 2001; Vol. 4345, p 19.

(17) Yolshina, L. A.; Kudyakov, V. Y.; Malkov, V. B.; Molchanova, N. G. Corrosion and Electrochemical Behavior of Aluminium Treated with High-Temperature Pulsed Plasma in CsCl-NaCl-NaNO3 Melt. *Corros. Sci.* **2011**, *53*, 2015−2026.

(18) Romero, K.; Stephan, R.; Grasshoff, G.; Mazur, M.; Ruelke, H.; Huy, K.; Klais, J.; McGowan, S.; Dakshina-Murthy, S.; Bell, S.; Wright, M. A Novel Approach for the Patterning and High-Volume Production of Sub-40-Nm Gates. *IEEE Trans. Semicond. Manuf.* **2005**, *18*, 539−544.

(19) Choi, S. J. Novel Spin-on Hard Mask with Si-Containing Bottom Antireflective Coating for Nanolithography. *J. Vac. Sci. Technol., B: Microelectron. Nanometer Struct.–Process., Meas., Phenom.* **2007**, *25*, 868−872.

(20) Zhu, D.; Liu, Y.; Yuan, L.; Liu, Y.; Li, X.; Yi, L.; Wei, H.; Yao, K. Controllable Synthesis of Large-Area Free-Standing Amorphous Carbon Films and Their Potential Application in Supercapacitors. *RSC Adv.* **2014**, *4*, 63734−63740.

(21) Lee, S.; Won, J.; Choi, J.; Park, J.; Jee, Y.; Lee, H.; Byun, D. Comparative Study on the Properties of Amorphous Carbon Layers Deposited from 1-Hexene and Propylene for Dry Etch Hard Mask Application in Semiconductor Device Manufacturing. *Thin Solid Films* **2011**, *519*, 6683−6687.

(22) Ho, C. Y.; Lin, X. J.; Chien, H. R.; Lien, C. High Aspect Ratio Contact Hole Etching Using Relatively Transparent Amorphous Carbon Hard Mask Deposited from Propylene. *Thin Solid Films* **2010**, *518*, 6076−6079.

(23) Lee, T.; Min, N. K.; Lee, H. W.; Jang, J. N.; Lee, D. H.; Hong, M. P.; Kwon, K. H. The Deposition of Amorphous Carbon Thin Films for Hard Mask Applications by Reactive Particle Beam Assisted Sputtering Process. *Thin Solid Films* **2009**, *517*, 3999−4002.

(24) Kim, H. T.; Kwon, B. S.; Lee, N.-E.; Park, Y. S.; Cho, H. J.; Hong, B. Etching Characteristics and Application of Physical-Vapor-Deposited Amorphous Carbon for Multilevel Resist. *J. Vac. Sci. Technol., A* **2008**, *26*, 861−864.

(25) Kim, J. K.; Il Cho, S.; Kim, N. G.; Jhon, M. S.; Min, K. S.; Kim, C. K.; Yeom, G. Y. Study on the Etching Characteristics of Amorphous Carbon Layer in Oxygen Plasma with Carbonyl Sulfide. *J. Vac. Sci. Technol., A* **2013**, *31*, No. 021301.

(26) Kim, K. J.; Park, J. J.; Lee, S. H.; Kim, S. I.; Park, Y. W.; Lee, C. G. An Enhancement of via Profile Using MLR Mask. *Microelectron. Eng.* **2011**, *88*, 2604−2607.

(27) Pears, K. A.; Stavrev, M.; Scire, A.; Koepe, R.; Markert, M.; Egger, U.; Donohue, L. Carbon Hard Masks for Etching Sub-90 Nm Structures. *Microelectron. Eng.* **2005**, *81*, 156−161.

(28) Guo, M.; Diao, D.; Yang, L.; Fan, X. Restructured Graphene Sheets Embedded Carbon Film by Oxygen Plasma Etching and Its Tribological Properties. *Appl. Surf. Sci.* **2015**, *357*, 771−776.

(29) Yu, L.; Sheeja, D.; Tay, B.; Chua, D. H. C.; Milne, W.; Miao, J.; Fu, Y. Etching Behaviour of Pure and Metal Containing Amorphous Carbon Films Prepared Using Filtered Cathodic Vacuum Arc Technique. *Appl. Surf. Sci.* **2002**, *195*, 107−116.

(30) Kwon, B. S.; Kim, J. S.; Lee, N. E.; Shon, J. W. Ultrahigh Selective Etching of SiO 2 Using an Amorphous Carbon Mask in Dual-Frequency Capacitively Coupled C 4 F 8 / CH 2 F 2 / O 2 /Ar Plasmas. *J. Electrochem. Soc.* **2010**, *157*, 135−141.

(31) Kim, J. K.; Lee, S. H.; Cho, S., Il; Yeom, G. Y. Study on Contact Distortion during High Aspect Ratio Contact SiO 2 Etching. *J. Vac. Sci. Technol., A* **2015**, *33*, No. 021303.

(32) Cho, H.; Hahn, Y. B.; Hays, D. C.; Jung, K. B.; Donovan, S. M.; Abernathy, C. R.; Pearton, S. J.; Shul, R. J. Inductively Coupled Plasma Etching of III-Nitrides in Cl 2 /Xe, Cl 2 /Ar AND Cl 2 /He. *MRS Proc.* **1998**, *537*, No. G6.56.

(33) Yoon, M. Y.; Yeom, H. J.; Kim, J. H.; Chegal, W.; Cho, Y. J.; Kwon, D.-C.; Jeong, J.-R.; Lee, H.-C. Discharge Physics and Atomic Layer Etching in Ar/C 4 F 6 Inductively Coupled Plasmas with a Radio Frequency Bias. *Phys. Plasmas* **2021**, *28*, No. 063504.

(34) Kofuji, N.; Ishimura, H.; Kobayashi, H.; Une, S. Mechanism of Wiggling Enhancement Due to HBr Gas Addition during Amorphous Carbon Etching. *Jpn. J. Appl. Phys.* **2015**, *54*, No. 06FH04.

(35) Oh, S.-J.; Sung, D.-Y.; Ko, J.-M.; Nam, S. K. Improving Detection of Plasma Etching End Point Using Light Compensation on Optical Emission Spectra. *J. Vac. Sci. Technol. B* **2022**, *40*, No. 052206.

(36) Mahi, B.; Arnal, Y.; Pomot, C.; et al. The Etching of Silicon in Diluted SF6 Plasmas: Correlation between the Flux of Incident Species and the Etching Kinetics. *J. Vac. Sci. Technol., B: Microelectron. Nanometer Struct.–Process., Meas., Phenom.* **1987**, *5*, 657.

(37) Kim, J. H.; Choi, S. C.; Shin, Y. H.; Chung, K. H. Wave Cutoff Method to Measure Absolute Electron Density in Cold Plasma. *Rev. Sci. Instrum.* **2004**, *75*, 2706−2710.

(38) Kim, J. H.; Seong, D. J.; Lim, J. Y.; Chung, K. H. Plasma Frequency Measurements for Absolute Plasma Density by Means of Wave Cutoff Method. *Appl. Phys. Lett.* **2003**, *83*, 4725−4727.

(39) Lee, M. H.; Jang, S. H.; Chung, C. W. Floating Probe for Electron Temperature and Ion Density Measurement Applicable to Processing Plasmas. *J. Appl. Phys.* **2007**, *101*, No. 033305.

(40) Bang, J. Y.; Yoo, K.; Kim, D. H.; Chung, C. W. A Plasma Diagnostic Technique Using a Floating Probe for the Dielectric Deposition Process. *Plasma Sources Sci. Technol.* **2011**, *20*, No. 065005.

(41) Choi, D.; Yeom, H. J.; You, K. H.; Kim, J. H.; Seong, D. J.; Yoon, E.; Lee, H.-C. Generation of Carbon Nanowhiskers, Nanotips, and Nanodots by Controlling Plasma Environment: Ion Energy and Radical Effects. *Carbon* **2020**, *162*, 423−430.

(42) Kwon, J. H.; Park, S. Y. L.; Seo, K. C.; Ban, W. J.; Park, G. O.; Lee, D. D. Relationship between Bonding Characteristics and Etch-Durability of Amorphous Carbon Layer. *Thin Solid Films* **2013**, *531*, 328−331.

(43) Kim, J.-H.; Chung, K.-H.; Shin, Y.-H. Analysis of the Uncertainty in the Measurement of Electron Densities in Plasmas Using the Wave Cutoff Method. *Metrologia* **2005**, *42*, 110−114.

(44) Yeom, H. J.; Kim, J. H.; Choi, D. H.; Choi, E. S.; Yoon, M. Y.; Seong, D. J.; You, S. J.; Lee, H.-C. Flat Cutoff Probe for Real-Time Electron Density Measurement in Industrial Plasma Processing. *Plasma Sources Sci. Technol.* **2020**, *29*, No. 035016.

(45) D'Agostino, R.; Cramarossa, F.; De Benedictis, S.; Ferraro, G. Spectroscopic Diagnostics of CF4-O2 Plasmas during Si and SiO2 Etching Processes. *J. Appl. Phys.* **1981**, *52*, 1259−1265.

(46) Morshed, M. M.; Daniels, S. M. Electron Density and Optical Emission Measurements of SF 6/O 2 Plasmas for Silicon Etch Processes. *Plasma Sci. Technol.* **2012**, *14*, 316−320.

(47) Lee, H. C.; Lee, M. H.; Chung, C. W. Low Energy Electron Heating and Evolution of the Electron Energy Distribution by Diluted O2 in an Inductive Ar/O2 Mixture Discharge. *Phys. Plasmas* **2010**, *17*, No. 013501.

(48) You, K. H.; Schulze, J.; Derzsi, A.; Donkó, Z.; Yeom, H. J.; Kim, J. H.; Seong, D. J.; Lee, H.-C. Experimental and Computational Investigations of the Effect of the Electrode Gap on Capacitively Coupled Radio Frequency Oxygen Discharges. *Phys. Plasmas* **2019**, *26*, No. 013503.

(49) Lieberman, M. A.; Lichtenberg, A. J. *Principles of Plasma Discharges and Materials Processing*; John Wiley & Sons, Inc.: Hoboken, NJ, USA, 2005.

(50) Rezaei, F.; Abbasi-Firouzjah, M.; Shokri, B. Investigation of Antibacterial and Wettability Behaviours of Plasma-Modified PMMA Films for Application in Ophthalmology. *J. Phys. D: Appl. Phys.* **2014**, *47*, No. 085401.

(51) Pandow, M.; Mackay, C.; Wolfgang, R. The Reaction of Atomic Carbon with Oxygen: Significance for the Natural Radio-Carbon Cycle. *J. Inorg. Nucl. Chem.* **1960**, *14*, 153−158.

(52) Vivensang, C.; Turban, G.; Anger, E.; Gicquel, A. Reactive Ion Etching of Diamond and Diamond-like Carbon Films. *Diam. Relat. Mater.* **1994**, *3*, 645−649.

(53) Montanari, C. C.; Miraglia, J. E. Electron-Impact Multiple Ionization of Ne, Ar, Kr and Xe. *J. Phys. B: At., Mol. Opt. Phys.* **2014**, *47*, No. 105203.

https://doi.org/10.1021/acsomega.3c02438
ACS Omega 2023, 8, 32450−32457